

Chapter 3: Optical Properties of Doped Semiconductors

3.1 - Introduction

Because thermoelectric materials require doping for optimization of the thermoelectric properties, understanding how free carriers in a material affect its optical absorption spectrum is quite important. Figure 3-1 illustrates several ways that free carriers affect the optical absorption edge spectrum. Region 1 involves absorption of light via plasma oscillation of the bulk free electrons, the magnitude of which depends on the free carrier concentration. Region 2, 3, and 4 are associated with interband transitions from the valence to conduction band, as indicated by the increase in absorption beginning around 0.28 eV. Region 2 precedes the onset of the absorption edge and is known as the Urbach tail, which is associated with randomly distributed impurities within the semiconductor. Regions 3 and 4 are associated with an increase or decrease in the band edge position, which occurs at high doping levels. The increase shown in Region 3 is known as the Burstein Moss shift, which occurs due to occupation of the conduction band edge upon heavy n-type doping. Region 4 indicates a decrease in the absorption edge energy (renormalization), which is thought to occur due to electron-electron repulsion. Each of these effects will be described in detail in the following sections.

The difference between the optical (Burstein-Moss shifted) and true band gaps have been studied in many material systems [47, 67, 68]. It is important to have an understanding of the Burstein Moss shifts and band gap renormalization for a variety of semiconductor device applications where both the majority and minority carrier concentrations and band energies are necessary to optimize performance. In thermoelectric materials, though, there is often no distinction made between the true and optical gaps in doped materials [69, 70]. While the differences can be circumvented in the case of an undoped material (PbTe undoped binary), some thermoelectric materials may include simultaneous shifts in the doping level and the band

structure during doping that we would like to characterize in the context of band engineering. In this thesis chapter, I quantify the Burstein-Moss shift to the optical gap, and gap renormalization in Iodine doped PbTe measured using DRIFTS. We use measured Seebeck coefficients to estimate the chemical potential (ξ), which is an improvement to simply measuring the Hall carrier concentration. Further, we attempt to improve upon renormalization estimates by self-consistently considering the band gap parameter for non-parabolic systems.

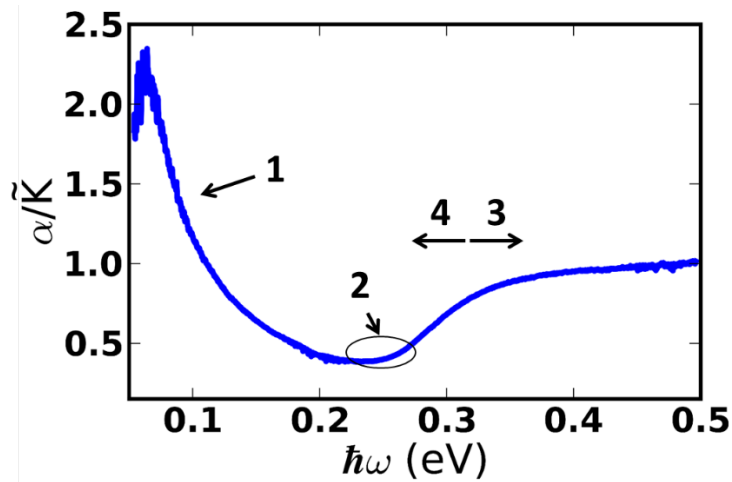


Figure 3-1: Optical absorption edge spectrum of an Iodine doped PbTe sample indicating the four regions that are present when considering optical processes relevant to free carriers: 1. Free carrier absorption, 2. Urbach edge, 3. increase in the interband transition energy (Burstein Moss Shift), and 4. band gap reduction as a result of doping (renormalization).

3.2 - Theory of Free Carrier Contributions to Optical Spectra

3.2a - Free Carrier Absorption

In n-type doped PbTe, a population of free carriers exists near the bottom of the conduction band, which can be excited to higher levels within the conduction via intraband transitions. The free electron cloud is perturbed by an incoming electric field, \mathbf{E} . Solutions to the Maxwell equations take the form of: $\mathbf{E} = \mathbf{E}_0 e^{i(\mathbf{k}\cdot\mathbf{r} - \omega\tilde{t})}$, (where \tilde{t} is the time), which yields the following form of the complex dielectric function ($\epsilon_c = \epsilon_1 + i\epsilon_2$) [43]:

$$\begin{aligned}\epsilon_c &= \epsilon_\infty + \frac{4\pi i}{\omega} \left(\frac{ne^2\tau}{m(1-i\omega\tau)} \right) \\ &= \epsilon_\infty \left(1 - \frac{\omega_p^2\tau^2}{1+\omega^2\tau^2} \right) + i \left(\frac{\epsilon_\infty\omega_p^2}{\omega(1+\omega^2\tau^2)} \right)\end{aligned}\quad \text{Equation 3-1}$$

Here, τ is the Drude scattering time and the plasma frequency is defined as $\omega_p = \sqrt{\frac{ne^2}{m^*\epsilon_\infty}}$.

Using this model for the complex dielectric function, it is straightforward to obtain both the real and imaginary components of the refractive index, which can then be used to obtain the frequency dependent reflectivity and absorption coefficient. In the case of specular reflection (perfect mirror reflection), the measured reflectivity can be compared to the result expected from the real and imaginary components of the refractive index, which can be derived from the dielectric function using [43]:

$$\epsilon_1 = n_r^2 - \kappa_r^2 \quad \text{Equation 3-2}$$

$$\epsilon_2 = 2n_r\kappa_r \quad \text{Equation 3-3}$$

and

$$R = \frac{(1 - n_r)^2 + \kappa_r^2}{(1 + n_r)^2 + \kappa_r^2} \quad \text{Equation 3-4}$$

which can be shown to yield a minimum in R near ω_p as a result of resonance between the photon and the bulk free electrons. The frequency at which the minimum occurs is roughly equal to ω_p (minor corrections have been shown by Lyden et al. [71]). In a diffuse reflectance spectrum, which is transformed by the Kubelka Munk function (Equation 2-1), this instead yields a maximum in $F(R)$. These maxima are observed in the more heavily doped PbTe samples ($n_H > 2 \times 10^{19} \text{ cm}^{-3}$) where the plasma frequency becomes larger than 0.05 eV as shown in Figure 3-2a. The measured peak in the Kubelka Munk function occurs even though the Praying Mantis diffuse reflectance instrument attempts to minimize the specular component of the reflection.

In terms of the absorption coefficient, α , (which Diffuse Reflectance attempts to capture), when $\omega \gg \tau^{-1}$: $\alpha_{FC} \propto \frac{ne^2}{n_r c m^* \tau \omega^2}$ where n is the number of free carriers, e is the elementary charge of an electron, n_r is the real refractive index, and c is the speed of light [43]. In order to isolate interband transitions, these features were fit and subtracted with a power law ($y = ax^b + c$). In almost all cases, the exponent, b , followed the expectation for Drude carriers of $b = -2$.

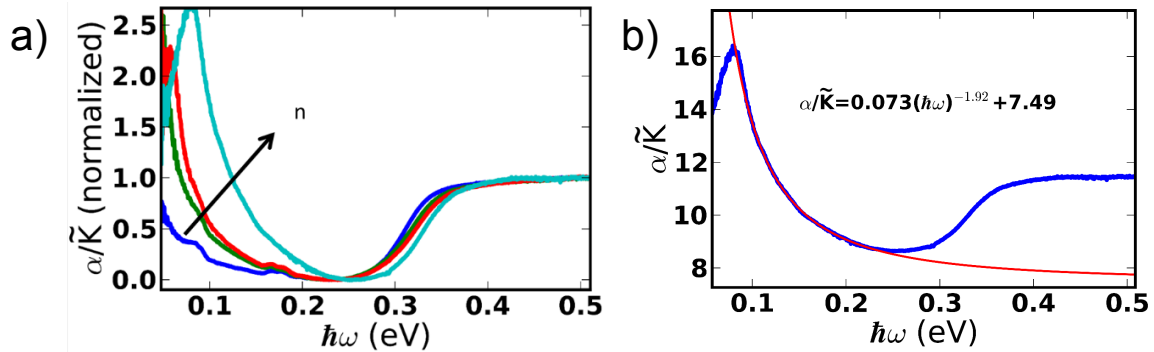


Figure 3-2: DRIFTS Spectra showing free carrier absorption contributions in Iodine doped PbTe. a) an increasing free carrier absorption with doping level, b) an example of a power law fit to the free carrier absorption.

3.2b - Urbach Edge

The second region of Figure 3-1 shows the exponential onset of absorption just below the fundamental absorption edge, known as the Urbach Edge (or Urbach tail). This effect is known to occur across a wide range of semiconductors, although ones with high impurity contents (or disordered alloys) have the largest Urbach tails (shown later in Chapter 4.3 for PbSe/SrSe alloys). The Urbach tail is thought to be related to the random distribution of impurity atoms in the material. For measurements done in this thesis, we also observe an approximately exponential increase in absorption just below the band edge [44, 45]. In this chapter, we will not treat the Urbach edge explicitly as we will attempt to fit the direct transitions instead, although its implications will be discussed.

3.2c - Burstein Moss Shift/Renormalization

Region 3, shown in Figure 3-1, indicates an upward shift in the absorption edge energy with doping. Heavily doped semiconductors (most good thermoelectric materials) have free carrier contributions to the optical absorption that can complicate the estimate of the band gap. In the case of degenerately doped semiconductors, this can cause large errors in the estimate of the true band gap on the order of the value of the chemical potential, ξ (which can be more than 0.1 eV in heavily doped samples). Since the early 1950's, it has been known that the measured optical band gap ($E_{g,opt}$) tends to change with increasing doping [72, 73]. These effects have even been considered in lead chalcogenides by some authors [74-77].

In the case of a degenerately doped n-type semiconductor, states near the conduction band edge become partially occupied. As a result, the photon energy required for excitation across a direct band gap becomes higher, increasing by $\left(1 + \frac{m_{cb}^*}{m_{vb}^*}\right)\xi$ in the case of direct transitions (where $m_{cb,vb}^*$ are the conduction and valence band effective mass respectively, see Figure 3-3). This results in an increase in the optical band gap ($E_{g,opt}$), known as the Burstein-Moss shift [45, 72, 75, 78]. The thermal gap, $E_{g,thermal} = E_g + \xi$, is relevant to transport properties and minority carrier excitation across the gap. The true band gap, E_g , has been shown both experimentally through optical measurements [47, 79, 80] and theoretically [47, 79, 80] to be reduced as the carrier concentration increases in heavily doped semiconductors, known as band gap renormalization (Δ_{RN})^{12,35-37}. Renormalization has been attributed to Coulombic repulsion of the electrons and/or exchange interactions. Thus, the optical band gap can be expressed as:

$$E_{g,opt} = E_g + \left(1 + \frac{m_{cb}^*}{m_{vb}^*}\right)\xi - \Delta_{RN} \quad \text{Equation 3-5}$$

which is illustrated in Figure 3-3.

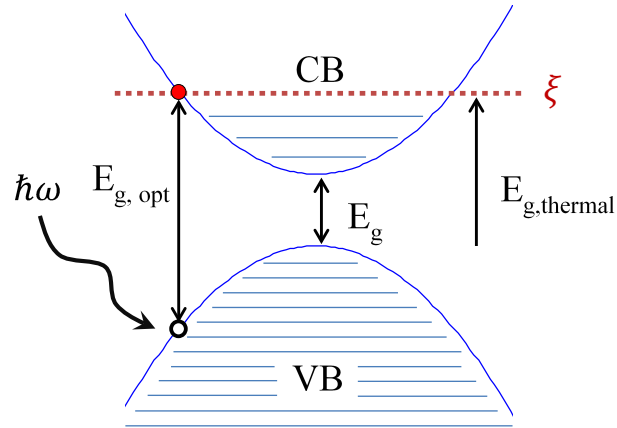


Figure 3-3: Optical excitations across the gap in a direct gap n-type degenerately doped semiconductor illustrating the Burstein-Moss shift and the different estimates of the band gap. Dashed line indicates the chemical potential, ξ .

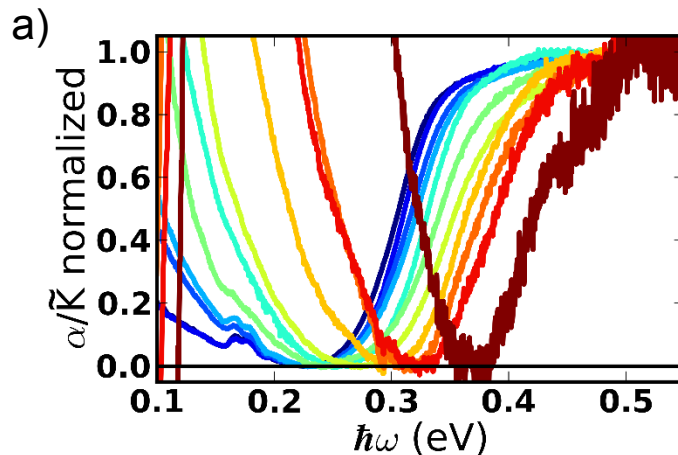
While the accepted view of PbTe is as a direct gap semiconductor, with evidence shown both experimentally [77, 81-83] and theoretically [84-86], some confusion existed in the early optical measurements. Some authors had also obtained good, linear fits to $\alpha^{1/2}$ vs. $\hbar\omega$ expected for indirect transitions [27, 37]. Similar to these reports, the absorption spectra in this thesis also provide a linear $\alpha^{1/2}$ vs. $\hbar\omega$ region where the extrapolated band-gap energy is slightly lower (~30-60 meV) than those fit for direct transitions. Scanlon suggests that this difference can be attributed to indirect transitions where a phonon is absorbed [37, 58], although single phonon energies are at most 12 meV or less based on a Debye temperature of 140 K [87] and neutron scattering experiments [88]. Prakash suggests Scanlon's observation could also be interpreted as merely a coincidental fit due to the Urbach tail (exponential decrease in density of states below the band edge) [39]. Although we believe that Prakash's interpretation is correct in PbTe, many materials do exhibit both indirect and direct transitions with some energy separation. For example, in germanium, both direct and indirect transitions exist with the indirect gap occurring first at about 0.63 eV and direct transitions beginning at 0.81 eV [89]. The indirect portion involves a slow rise in absorption coefficient over a long energy range ($\sim 100 \text{ cm}^{-1}$ over $\sim 0.2 \text{ eV}$) while the direct absorption on the other hand gives a much steeper rise over a shorter period ($\sim 10^4 \text{ cm}^{-1}$ over $\sim 0.05 \text{ eV}$). As a result, the direct gap is much more easily observed, particularly if both direct and

indirect transitions occur at close to the same energies. The absorption coefficient of PbTe changes $\sim 10^4 \text{ cm}^{-1}$ over $\sim 0.05 \text{ eV}$ [76, 90], suggesting that it is a direct gap semiconductor.

Recently, it has been suggested that the true gap value is convoluted by mid-gap defect states [91]. While these states may affect the measured optical band gap, we see no significant contribution from localized states in the transport properties; transport measurements are characteristic of itinerant (delocalized) carriers giving metal-like transport behavior (implying that the suggestion of mid-gap states is incorrect). Therefore, the measured absorption edge was assumed to be associated with the band edge in PbTe and not mid gap defect states, although defect states near the band edge could certainly play a role in band gap renormalization.

3.3 - Results and Discussion

Figure 3-4a shows the raw absorption spectra for a series of Iodine doped PbTe samples. A steady shift in the absorption edge to higher energies is observed with an increase in dopant concentration. Upon fitting and subtracting the free carrier absorption portions at low energies and applying the Tauc transformation for direct gaps, the gaps can be extrapolated as shown in Figure 3-4b. The results of the extrapolations are plotted (Figure 3-4c) as the optical band gap ($E_{g,opt}$) as a function of charge carrier concentration for Iodine and Lanthanum doped PbTe and Bromine doped PbSe.



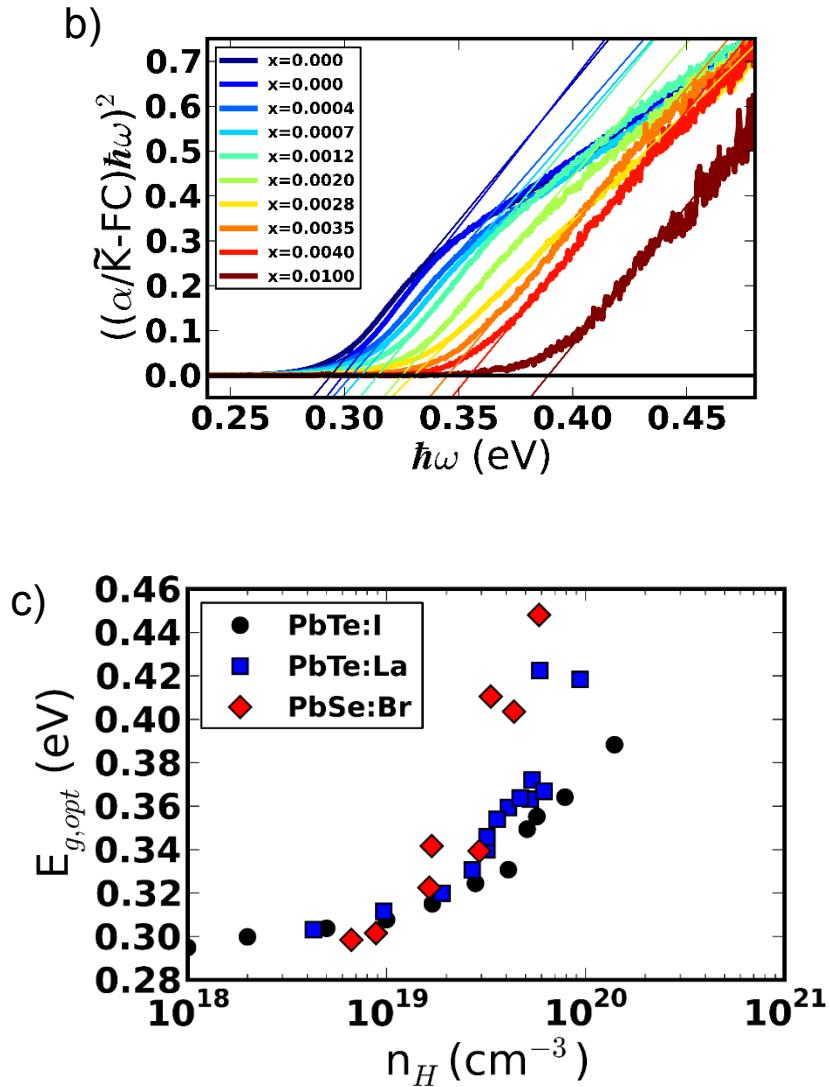


Figure 3-4: Normalized Kubelka Munk function for $PbTe_{1-x}I_x$ for a) raw data, and b) absorption coefficient direct gap extrapolation using the Tauc method. c) the resulting optical band gaps for n-type PbTe doped w/ either Iodine or Lanthanum and PbSe doped with Bromine.

Figure 3-4 clearly shows the increasing optical band gap with doping level; in order to quantify this effect, ξ must be determined. In many cases, the chemical potential is estimated by the 0 K limit of the parabolic band (Fermi energy, E_F): $E_F = \frac{\hbar^2}{2m^*} (3\pi^2 n)^{2/3}$ [68, 92, 93]. While this may be a good estimate for degenerate systems (at low temperature, high doping) with parabolic band shapes, a better estimate involves solving the more general temperature-dependent expression, $n = \int_0^\infty D(E)f(E,\xi,T)dE$, where D is the density of states and f is the Fermi

distribution function. It is well known that many semiconductors, including lead chalcogenides, deviate significantly from parabolic behavior. Ravich has developed an adaptation of the Kane band model for application to the lead chalcogenides, which has shown excellent agreement to experimental transport data [16, 28, 58]. Using Ravich's solution of the Kane band model applied to lead chalcogenides, n can be calculated by numerically integrating Equation 3-6:

$$n = \frac{(2m^*k_B T)^3}{3\pi^2\hbar^3} {}_0F_0^{3/2} \quad \text{Equation 3-6}$$

where $m_{d,0}^*$ is the band edge density of states effective mass, ϵ is the dimensionless energy ($\epsilon = \frac{E}{k_B T}$), β is the non-parabolicity parameter ($\beta = \frac{k_B T}{E_g}$ from Ravich), η is the reduced chemical potential $\eta = \frac{\xi}{k_B T}$, and $n_{F_l}^m = \int_0^\infty \left(-\frac{df}{d\epsilon}\right) \epsilon^n (\epsilon + \beta\epsilon^2)^m [(1 + 2\beta\epsilon) + 2]^{1/2} d\epsilon$ (a modified version of the Fermi integrals, Equation 2-17, from Wang et al [65]). The band gap parameter in the Kane model was assumed to have a constant value equal to that of the undoped PbTe, 0.295 eV, for this analysis. Calculation of the chemical potential as a function of the true carrier concentration is rather straightforward, but in order to compare to the Hall carrier concentration the Hall factor, r_H , is needed [58, 65]:

$$r_H = \frac{3K(K+2)}{(2K+1)^2} \frac{{}_0F_0^{1/2} {}_0F_0^{3/2}}{({}_0F_{-2}^1)^2} \quad \text{Equation 3-7}$$

where K (as defined in Chapter 2) is the anisotropy factor ($K = \frac{m_{\parallel}^*}{m_{\perp}^*} = 3.58$ [16]). By combining Equation 3-6 and Equation 3-7 to obtain $n_H = n/r_H$, we can plot the chemical potential dependent carrier concentration in Figure 3-5b (blue line) for $m_{d,0}^* = 0.276 m_e$.

Alternatively, using the Boltzmann transport equation, it is possible to obtain an estimate for the chemical potential, ξ , directly from the measured Seebeck coefficient with no assumption about the band edge effective mass (Equation 3-8) [58, 65]. The raw Seebeck data as a function of Hall carrier concentration is plotted in Figure 3-5a along with an S vs n_H (Pisarenko plot)

estimate using the SKB model (Red line derived using Equation 3-6, Equation 3-7, and Equation 3-8).

$$S = \frac{k_B}{e} \left(\frac{{}_1F_{-2}^1}{{}_0F_{-2}^1} - \eta \right) \quad \text{Equation 3-8}$$

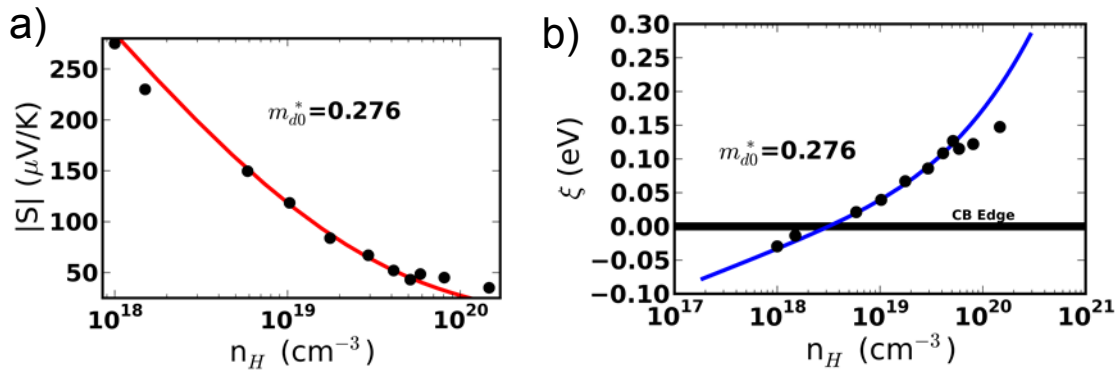


Figure 3-5: a) Seebeck Pisarenko plot for PbTe:I with the SKB model curve ($m_{d0}^* = 0.276$) shown. b) The change in electrochemical potential (calculated from the Seebeck coefficient) with Hall carrier concentration as a result of doping.

Figure 3-5b shows the calculated chemical potential for each iodine doped sample calculated using a single Kane band model both from the room temperature Seebeck measurements (solid points) along with the result assuming $m_{d0}^* = 0.276 m_0$ (best fit of the Seebeck vs. n_H Pisarenko plot). Here, we can see the chemical potential for the most heavily doped samples increases to ~ 0.15 eV from the band edge. It is important to note that the chemical potential estimate can vary significantly depending on the particular band model. In the case of a single parabolic band, the chemical potential can change to be as much as 50% higher for the same doping level and effective mass (this is a consequence of the Kane band effective mass increasing with increasing ξ). Once ξ is known, it is possible to estimate the true gap from the optical gap measurement (Figure 3-4). As an alternative to the Tauc method, the gap can also be fit using the spectral Fermi distribution.

The Fermi distribution can be projected onto the unperturbed interband absorption as a multiplicative factor, shown in Equation 3-9. This technique and similar methods have been

performed on a variety of materials, including lead chalcogenides [75, 76] and other materials [47, 67, 72, 94].

$$\alpha(\hbar\omega) \propto \alpha_0(\hbar\omega) [1 - f(\hbar\omega, \zeta, T)] \quad \text{Equation 3-9}$$

Here, α_0 is the absorption for an unpopulated conduction band at $T = 0$ K, which for parabolic

bands is proportional to $\alpha_0 = \frac{\sqrt{\hbar\omega - E_g}}{\hbar\omega} = \frac{\sqrt{\hbar\omega - [E_{g,opt} - (1 + \frac{m_c^*}{m_{vb}^*})\xi]}}{\hbar\omega}$. f is the Fermi distribution, which is

related to the photon energy as $f(\hbar\omega, \xi, T) = \left[1 + \exp\left(\frac{\hbar\omega - E_{g,opt}}{(1 + \frac{m_c^*}{m_{vb}^*})k_B T}\right) \right]^{-1}$. The second term in

Equation 3-9 represents the electronic excitation probability based on the electron population from Fermi distribution.

Using the proportionality factor and the band gap value as a fitting parameter, it is possible to obtain an estimate for the optical band gap using Equation 3-9 from the measured absorption spectra for a given estimate of the chemical potential, ξ (as estimated from either room temperature Seebeck and n_H measurements). A resulting fit of the absorption spectrum is shown in Figure 3-6. The Fermi projection method gives the optical band gap near the inflection point in the absorption (where the slope is the largest) which agrees approximately in trend obtained directly from extrapolation (Figure 3-7a) using the Tauc method (although is ~ 0.01 - 0.02 eV higher in energy than the Tauc extrapolation method). Results regarding the Fermi broadening method are included in a separate work on the subject [95], but in the remainder of this thesis I will only present results using the Tauc extrapolations (Figure 3-4).

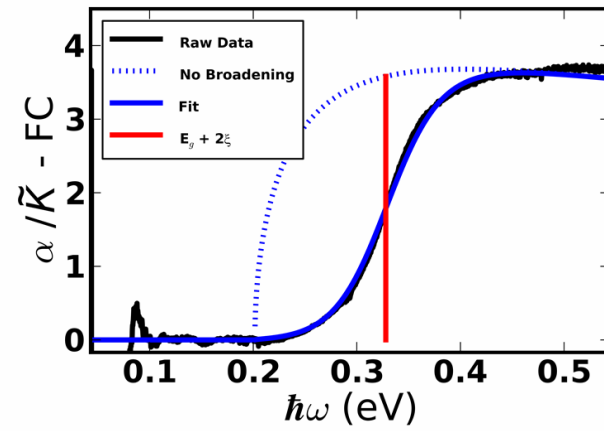


Figure 3-6: Fermi spectra method projecting the Fermi distribution onto the absorption edge in $PbTe_{1-y}I_y$, $y = 0.0012$ fit with a Fermi function.

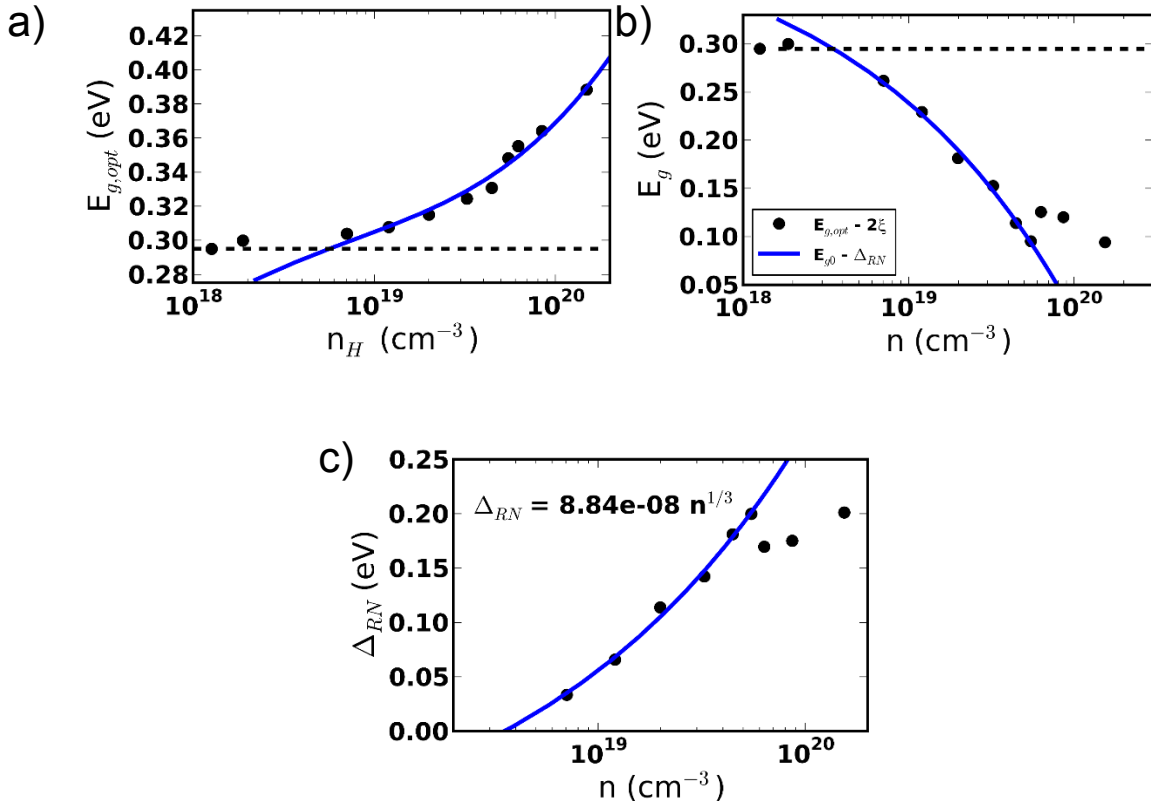


Figure 3-7: a) Optical band gaps fit from optical data via extrapolation by the Tauc plot method along with the curve fit from Equation 3-5. b) The true band gap, calculated from the optical gaps by $E_g = E_{g,opt} - 2\xi$ and the curve, which is given by $E_g = E_{g,0} - \Delta_{RN}$. c) Band gap renormalization fit: experimental data is $\Delta_{RN} = E_{g,0} - (E_{g,opt} - 2\xi)$, and the curve is given by the best fit: $\Delta_{RN} = An^{1/3} + \Delta_{RN,0}$.

Figure 3-7a shows an increasing optical gap with doping level, known as a Burstein-Moss shift. As the doping level increases, the chemical potential in the conduction band moves upward, which creates occupied states nearest the band edge, requiring a higher energy photon for excitation of a carrier across the gap. Following Figure 3-3 (and Equation 3-5) we can relate the optical gap to the true gap, E_g .

Figure 3-7b shows the calculated true band gap with respect to doping level. In the case of direct transitions and similar valence and conduction band effective masses, the true band gap is related to the optical gap and the chemical potential as $E_g = E_{g,opt} - 2\xi$. The result shows a true gap that decreases significantly with doping level relative to the undoped sample. This is a

result of the measured optical gap not increasing as quickly as expected based on the calculated ξ . Over the same doping range, the optical band gap is expected to increase by 2ξ , which is as much as 0.25 eV at the highest doping levels (see Figure 3-5b). The measured optical band gap, however, only increases by about 0.1 eV (about 40% of ξ) at the highest doping levels, as shown in Figure 3-4c/Figure 3-7c/Table 3-1. The relatively small change of the optical band gap can be explained by the renormalization effect, which is an estimate of band gap shrinkage with doping.

The true band gap in Equation 3-5 can also be represented by $E_g = E_{g0} - \Delta_{RN}$, which accounts for a shrinking band gap with increasing doping level as shown in Figure 3-7b. Both experimental and theoretical work has been done to determine how the band gap should shrink due to renormalization with increasing electron concentration in many semiconductors, including Si [47, 67, 80, 96, 97], Ge [96, 98], GaAs [68, 99], InP [79], ZnO [100], and other materials. The effect has proven important in semiconductor device applications where the material's band gap determines many device characteristics and careful engineering is required to optimize performance. Gap narrowing is thought to be due to a combination of effects, including electron-electron exchange interactions, electron-donor interactions, and band tailing [92, 96, 99, 101]. Electron-electron exchange has been shown to scale as $n^{1/3}$ in a weakly interacting free electron gas [96, 100]; this model is often used empirically, although the specific form may vary with crystal and energy band structure. The effect can be thought of as Coulombic repulsion between free electrons in the material, which scales as $1/r$ where r is the mean distance between electrons. Experimentally, attempts have been made to empirically fit the theoretical models. Most use a combination of power laws whose prefactors can in theory be calculated, but are most often used as fitting parameters [92, 96, 101]. Drabkin et al., for example, suggest that for PbTe a shift on the order of 10 meV is reasonable for doping levels on the order of $1 \times 10^{19} \text{ cm}^{-3}$ [76]. When using the method of Mahan [101], however, the predicted reduction is actually 1 meV or less due to the large static dielectric constant ($\epsilon(0) \approx 400$) for PbTe. Following other references [47, 67], I fit the

experimental renormalization to an $n^{1/3}$ power law, including an additional constant term: $\Delta_{RN} = An^{1/3} + \Delta_{RN,0}$. The resulting renormalized fits to the optical and true band gap are plotted in Figure 3-7a and b and are also shown in Table I. Figure 3-7c shows the fitting result for the band gap renormalization. Note that the renormalization does not become non-zero until ξ becomes greater than the conduction band edge ($n > 3 \times 10^{18} \text{cm}^{-3}$), which is likely the origin of the $\Delta_{RN,0}$ term.

As mentioned previously, Figure 3-7b shows that the true band gap is rather significantly reduced at high doping levels due to renormalization. For the three most heavily doped samples, ξ , as estimated from Seebeck coefficient measurements, does not continue to increase at the same rate. As a result, the true gap approaches an approximately constant value of close to 0.12 eV. The $n^{1/3}$ model (blue curve Figure 3-7c) deviates significantly for carrier concentrations $> \sim 6 \times 10^{19} \text{cm}^{-3}$, resulting in an estimated gap (blue curve in Figure 3-7b) that rapidly approaches zero above this value. While the magnitude of the gap reduction is consistent with previously published results for heavily doped n-type PbTe [76], Si [47, 67, 80], Ge [98], and III-V semiconductors [68, 79, 92, 99, 102], the apparent discrepancy at high doping is not easily explained using the simple $n^{1/3}$ empirical model.

Table 3-1: Band gap and transport measurement results and chemical potential estimates for this series of samples. All Kane band calculations assume a constant β parameter of ~ 0.087 corresponding to the undoped sample band gap of 0.295 eV. Chemical potentials are presented for the experimental results (ξ_{Seeb}) and model curve fit (ξ_{SKB}) as shown in Figure 3-5b.

x	n_H (10^{18}cm^{-3})	S ($\mu\text{V/K}$)	ξ_{Seeb} (eV)	$\xi_{\text{SKB}}(m^*=0.276)$ (eV)	$E_{g, \text{opt}}$ (eV)	$\Delta_{\text{RN,Seeb}}$ (eV)
0.0000	-	-275.0	-0.030	-0.033	0.295	-
0.0000	-	-230.0	-0.014	-0.022	0.300	-
0.0004	5.87	-141.4	0.021	0.020	0.304	0.033
0.0007	1.03	-109.6	0.039	0.040	0.308	0.066
0.0012	1.76	-81.9	0.067	0.063	0.315	0.114
0.0020	2.94	-66.9	0.086	0.089	0.324	0.142
0.0028	41.1	-52.0	0.108	0.108	0.331	0.181
0.0035	51.4	-43.0	0.126	0.123	0.349	0.199
0.0040	58.7	-42.9	0.115	0.132	0.355	0.170
0.0055	80.8	-41.5	0.122	0.156	0.364	0.175

0.0100	147	-33.7	0.147	0.208	0.388	0.201
--------	-----	-------	-------	-------	-------	-------

In Ravich's adaptation of the Kane band model for lead chalcogenides, the band gap is a necessary parameter as it determines the non-parabolicity parameter: $\beta = \frac{k_B T}{E_g}$. Because optical measurements have shown evidence that the band gap in PbTe decreases with doping as a result of band gap renormalization, it might be expected to affect the band structure. The band edge effective mass in narrow gap semiconductors has been suggested to scale with the band gap itself [43, 58]. Ravich suggests that the energy dependent effective mass for a Kane type band should scale with energy as:

$$m^*(E) = \frac{\hbar^2 E_g}{2P^2} \left(1 + \frac{2E}{E_g} \right) \quad \text{Equation 3-10}$$

where P is the $k \cdot p$ matrix element coupling states between the valence and conduction band states. The first term in Equation 3-10 will scale proportional to the band gap, while the second will scale with E , the electron energy. More often, the prefactor in Equation 3-10 is treated as a constant, m_0^* , the band edge effective mass, which can be fit from the Seebeck coefficient vs. carrier concentration Pisarenko plot. Because m_0^* appears to be independent of carrier concentration, we will only consider the effect of the changing band gap with carrier concentration through the β parameter. In order to probe the effect that this might have on the estimate of ξ and on the transport properties, a self-consistent approach should be taken.

For all of the previous calculations, ξ has been estimated from Seebeck coefficient (Equation 3-8) assuming a constant Kane-band non parabolicity parameter (β used in Equation 3-6 and Equation 3-8) given by assuming a constant band gap of 0.295 eV equal to that of the undoped PbTe sample. Using the fitted n -dependent gap, $E_g(n) = E_{g0} - \Delta_{RN}(n)$, we can self-consistently calculate n as a function of chemical potential with an n -dependent nonparabolicity

parameter, $\beta = \frac{k_B T}{E_g(n)}$. The new value of chemical potential was used to recalculate the gap renormalization using the measured optical gaps, which was again fit to an $n^{1/3}$ model. After several iterations, the true gap appeared to converge to a self-consistent value that was slightly higher than the previous result which assumed constant gap. The self-consistent solution yielded renormalization fitting parameters of 5.6×10^{-8} eV-cm and -0.068 eV for A and $\Delta_{RN,0}$ respectively. The band gap, both fit (solid lines) and values from measurements (circles), for the model assuming either constant β or an n -dependent band gap (self-consistent) are shown Figure 3-8a. Renormalized gap estimates were obtained using measured optical gaps and estimates of the chemical potential, ξ (shown in Figure 3-8b). Here, we can see the effect of the band-nonparabolicity as an increasing band mass (which increases even faster as a result of the increasing $\beta(n)$) as the chemical potential rises. At higher carrier concentrations ($> 6 \times 10^{19} \text{ cm}^{-3}$), the renormalized band gap value becomes quite small, and errors become larger. Therefore, the fact that $E_g(n)$ levels out at about 0.15 eV may not be entirely accurate since the renormalization effect is probably overestimated at these doping levels. Further, PbTe is known to deviate from the Kane model for carrier concentrations greater than this value [103]. As in the constant β case, the empirical $n^{1/3}$ model may be an oversimplification in the case of increasingly narrow gap and/or the simplified Kane model of Ravich may also be an oversimplification that cannot account for these narrowing phenomena.

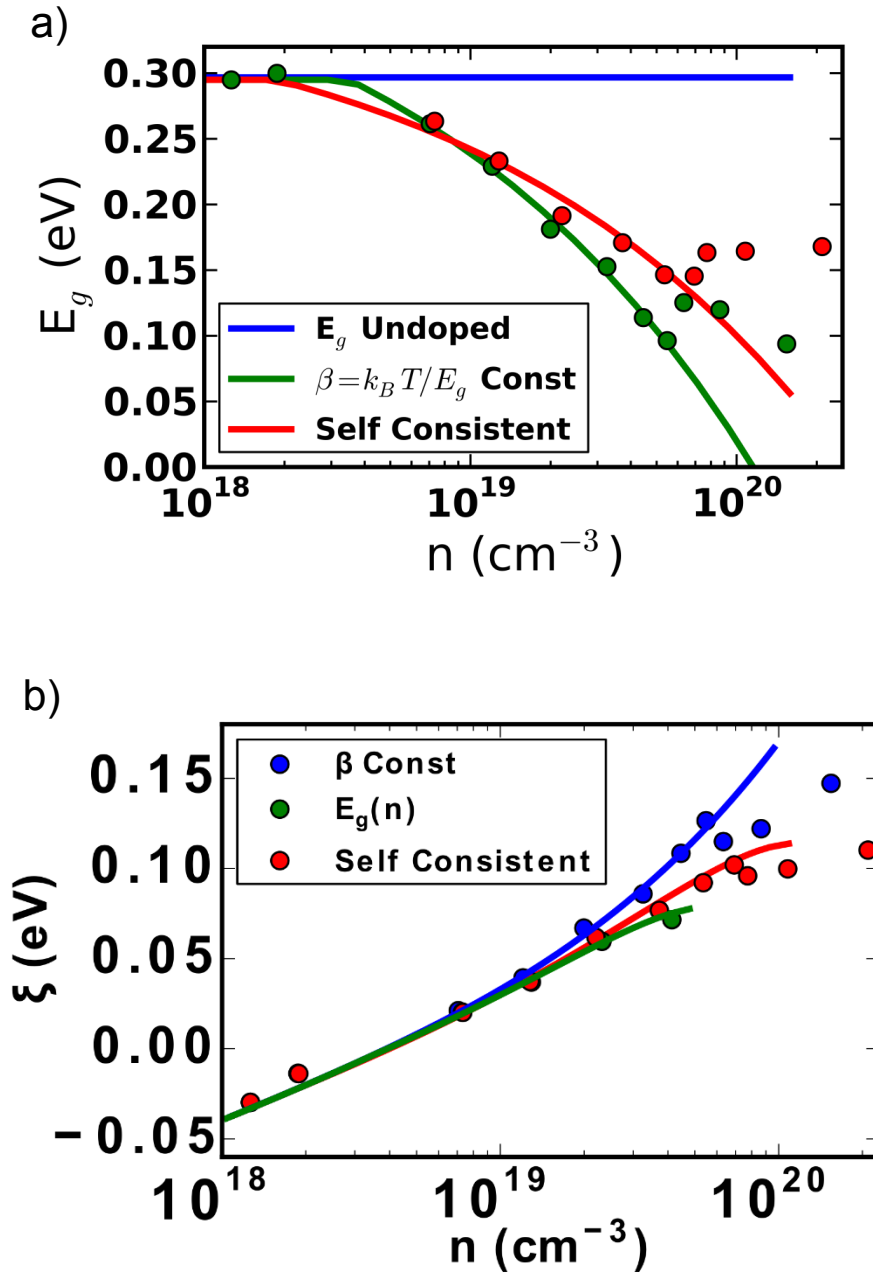


Figure 3-8: Iterative self-consistent calculation of the true gap $E_g(n)$ in accordance with the Kane band model. a) The result of different n -dependences of the Kane β parameter solid points represent $E_g(n)$ in accordance with eq. 5 (using the measured optical gaps and chemical potential estimates from Seebeck coefficient measurements). b) The estimated chemical potential as a function of doping level for different dependence of β on n ; lines represent constant effective band edge mass (Eq 3, $m^*_0 = 0.276 m_0$) and points are calculated from Seebeck coefficient (Equation 3-8).

In the discussion of electronic band structure it is typically a good first approximation to assume the energy bands remain unaltered with doping, which is known as the rigid band approximation. Lee, Mahanti et al. give some examples where this may not be a good assumption

in Na doped PbTe [104], although the picture here is complicated by the variability in supercell calculations [105]. Experimental measurements of effective mass can show small changes in band structure when using different dopants (I or La) in PbTe, which may be related to a shift in band gap [106]. With the goal of band engineering in mind it is important to be able to determine how the band structure is altered as the materials are doped or alloyed. While the rigid band approximation works reasonably well for many purposes, this work demonstrates that the differences between true, optical, and thermal band gaps can be different of the order 0.1 eV (which is quite large considering that the true gap is ~ 0.3 eV). Most thermoelectric materials are heavily doped semiconductors, where $E_{g,thermal} \gg k_B T$. In this case, the electronic transport properties (electrical conductivity, Seebeck coefficient) are determined by a single band. The most obvious effect of a narrower band gap is the increased concentration of minority carriers. In the case of most thermoelectric materials, though, the chemical potential (and thermal band gap) is deep enough into the band to where the minority carrier population is still very small compared to majority carriers. The effects become more apparent at high temperatures when $k_B T \sim E_{g,th}$.

While band gap renormalization is a well-known effect that has been studied in many materials, it is generally ignored in thermoelectric materials in favor of the rigid band approximation. This work suggests that in PbTe, both approximations may play a role. While it seems unlikely that the band gap in these materials might become very small (or even approach zero), it is possible that if the material is sufficiently doped that bipolar effects can be suppressed and a reduced band gap would not be observed by measuring transport properties alone.

Ultimately, the apparent discrepancy between the rigid band approximation and band gap renormalization may need to be resolved with either better estimates of the n -dependent chemical potential, or by developing models that more accurately represent renormalization in narrow gap semiconductors. Perhaps more experimental and theoretical work should be done to investigate what is different in narrow gap, heavily doped semiconductors from other wider gap materials.

3.4 - Conclusions

While the DRIFTS method of measuring the optical absorption has been thoroughly explored in catalysis research and has shown some promise for quantifying chemical reactions [107, 108], as a technique for precisely determining band gaps in semiconductors diffuse reflectance has only proven semi quantitative (± 0.1 eV) [109]. In this work, we detect shifts in band gap with doping of smaller than 0.01 eV in PbTe, which can be analyzed and understood by methods consistent with current optical literature.

While electronic transport measurements are essential to determine the thermoelectric properties for a materials, optical properties can provide more direct knowledge about the band structure. Although diffuse reflectance measurements have been used in the thermoelectric literature, it is important to account for the effects of electron population on the absorption edge that alters the observed optical band gap. I have shown a series of iodine doped PbTe samples which show a Burstein-Moss shift in the absorption edge to higher frequencies. Using estimates of the chemical potential from transport measurements, it is possible to estimate that a gap shrinkage of up to 0.15 eV occurs at the highest doping levels appropriate to thermoelectrics. An attempt is made to fit the true gap self-consistently using a single band Kane model, which results in a slight reduction in the renormalization. While renormalization has been shown to fit well-behaved empirical models for many semiconductors, PbTe (and possibly other narrow gap materials) exhibits a Burstein-Moss shift and renormalization that are not readily explained with existing theory.

Ultimately, even though the effects of doping on the value of the band gap can be accounted for using the Burstein Moss shift and renormalization effects, measuring undoped samples is preferred when trying to distinguish small shifts due to temperature or alloying. But, because it is not always possible to make undoped samples due to intrinsic defects, it is important

to be able to recognize the effects of doping on optical absorption edge measurements and to be able to account for differences that they may cause.